TU Delft

Delft University of Technology

Stability Region Exploring of Shunt Active Power Filters Based on Output Admittance Modeling

Lei, Jintao; Qin, Z.; Li, Wuhua; Bauer, P.; He, Xiangning

DOI
10.1109/TIE.2020.3044750

Publication date
2021

Document Version
Accepted author manuscript

Published in
IEEE Transactions on Industrial Electronics

Citation (APA)
Lei, J., Qin, Z., Li, W., Bauer, P., & He, X. (2021). Stability Region Exploring of Shunt Active Power Filters Based on Output Admittance Modeling. *IEEE Transactions on Industrial Electronics*, *68*(12), 11696-11706. Article 9301372. https://doi.org/10.1109/TIE.2020.3044750

Important note
To cite this publication, please use the final published version (if applicable).
Please check the document version above.

Copyright
Other than for strictly personal use, it is not permitted to download, forward or distribute the text or part of it, without the consent of the author(s) and/or copyright holder(s), unless the work is under an open content license such as Creative Commons.

Takedown policy
Please contact us and provide details if you believe this document breaches copyrights.
We will remove access to the work immediately and investigate your claim.

This work is downloaded from Delft University of Technology.
For technical reasons the number of authors shown on this cover page is limited to a maximum of 10.

Stability Region Exploring of Shunt Active Power Filters Based on Output Admittance Modeling

Jintao Lei, *Student Member, IEEE*, Zian Qin, *Senior Member, IEEE*, Wuhua Li, *Member, IEEE*, Pavol Bauer, *Senior Member, IEEE* and Xiangning He, *Fellow, IEEE*

***Abstract*—Shunt Active Power Filter (SAPF) is coupled with load admittance in weak grid conditions, which poses a challenge to stability analysis. In this paper, the admittance model of the SAPF is developed, which reveals the coupling mechanism between SAPF and load concisely and accurately. On top of that, the stability region of the system is investigated. Passivity region of the load admittance to guarantee the system stability is firstly explored. However, Passivity region has very narrow band at a specific frequency, which makes it difficult to achieve. Stability region is then studied and it turns out to be an extension of the passivity region, and especially the narrow band is expanded. Therefore the stability region is much easier to meet. The stability-oriented design is then summarized in a flow chart. In the end, the effectiveness of the newly defined stability region is verified by experimental results.**

***Keywords*—active power filters, stability, admittance, modeling**

I. Introduction

Power electronics, which is used at both the generation and demand sides for high conversion efficiency, is experiencing a rapid growth [1-4]. Dc grid technology was proposed in recent years, which has the advantage of effectively integrating those dc power sources and loads. Despite this, the ac grid is still dominating the power system. In the ac grid, most of the electrical loads like adjustable speed drives, power supplies, electrolyzers, etc. [5, 6], have a front-end rectifier to convert AC grid voltage to DC voltage to fulfill the requirement of the loads. The rectifiers, especially the passive ones, cause significant power quality (PQ) issues, in terms of harmonic currents [7, 8]. The harmonic currents cause more cable loss, lead to grid voltage distortion and thereby speed up the aging of the cable and transformer insulators, etc. Moreover, it degrades the performance of the protection equipment in the power system, e.g., relays, circuit breakers, etc.

According to the utility harmonic standards, such as IEEE Standard 519-1992 and IEC Standard 61000-3-6, the total harmonic distortion (THD) in the current of the grid-connected device should be lower than 5%. To fulfill the standard, passive RLC power filters (PPFs), are widely used in demand-side and distribution system [9, 10]. However, the PPFs have significant drawbacks, including heavyweight, non-flexibility, self-resonance, etc. In contrast, the shunt active power filter (SAPF) has been proved to be a superior solution for harmonics current mitigation due to its smaller size, better dynamic performance, and more flexibility [11, 12]. Since SAPF is used for compensating load harmonic currents, it is common to simplify the load into a harmonic current source in the modeling of SAPF [13-16]. Research effort has been mainly put on current control strategies [17-22], topologies [23-25], and reference current extraction methods [26-28] to enhance the harmonic compensation performance. It takes for granted to consider SAPF to be in favor of system stability by eliminating harmonic currents. However, it might not be true when the load dynamic is not taken into consideration.

The impact of SAPF on grid stability has been studied in a few pieces of literature. A new model for SAPF was proposed in [29], where the influence of the load and grid impedance were considered. On top of the proposed SAPF model, stability analysis was performed, and a damping approach was applied to suppress resonance. Yet, SAPF was modeled as a voltage source in series with an *LCL* filter, which has some gap with reality. The model was further developed in [30], where the interaction between the load and APF was considered into one integrated model. However, all effects are coupled together, so it is challenging to study the influence of load and SAPF individually. A Lyapunov stability theory-based control method was proposed for a three-level SAPF in [31], which does not rely on linearization of the system. However, with the minimal details provided in the literature, it is hard to tell how the control and load influence the stability.

Impedance based approach has been proved to be useful in analyzing the interactions of converters [32-34]. Among the different small-signal methods for stability analysis of power electronics-based grid, the impedance-based approach is superior in terms of design-oriented analysis, modularity, and scalability [35, 36]. Therefore, to reveal the impact of SAPF on the stability of the grid, a concise and accurate SAPF output admittance model was developed in our previous work [37], considering the influence of the load dynamic. In this paper, the admittance modelling is presented in a more concise way. More importantly, based on the developed admittance model of SAPF, the stability region of the system is investigated. Passivity region of the load admittance to guarantee the system

This work was supported by the National Key Technologies R&D Program of China under Grant 2017YFE0112400, and the European Union's Horizon 2020 research and innovation programme under Grant agreement No 734796. (Corresponding Author: Zian Qin)

J. Lei, W. Li and X. He are with the College of Electrical Engineering, Zhejiang University, Hangzhou 310027, China. (leijintao@zju.edu.cn, woohualee@zju.edu.cn, hxn@zju.edu.cn)

Z. Qin and P. Bauer are with the Department of Electrical Sustainable Energy, Delft University of Technology, 2628 CD Delft, Netherlands. (z.qin-2@tudelft.nl, P.Bauer@tudelft.nl)

stability is firstly explored. However, Passivity region has very strict boundary conditions, which are difficult to achieve in reality. Stability region is then studied and it turns out to have much less strict boundary conditions, and thereby much easier to fulfill. The stability region defined in this paper provides a guide to SAPF for valid application scenarios, where accurate admittance model of the load is not required, instead a rough knowledge of the admittance is sufficient to judge the stability of the system. A stability-oriented design is summarized in a flow chart. The rest of this paper is organized as follows: in Section II, the modeling of SAPF takes the load dynamics into account, and a frequency-sweep verifies it; Section III explores the stability region based on the developed admittance model; Section IV performs the experimental validation; Section V concludes the paper.

II. Impedance Modeling

A. Modeling

Fig.1 shows a three-phase grid-connected system, including the load, SAPF, and grid. The grid is simplified into a voltage source V_g in series with impedance $Z_g(s)$ that composed of L_g and R_g. The load and SAPF are connected to the Point of Common Coupling (PCC), where the voltage is defined as V_{pcc}, in parallel. In SAPF, an *LCL* filter composed of L_1, L_2, and C_f is applied to achieve a relatively smaller filter size and the voltage near the inverter side is defined as V_{inv}. The control diagram of the SAPF is shown in Fig. 2. To compensate for the harmonic items in the load current, the load current I_L is firstly measured. Then by employing a high pass filter $G_{hp}(s)$, the harmonic items in I_L are extracted. Since the positive direction of I_L is defined as from load to grid, the current reference I_{ref} of the current controller in SAPF has the same amplitude as harmonic items in I_L but in the opposite phase. Note that the control of dc-link voltage V_{dc} and phase-locked loop (PLL), are not considered. As known, the dc-link voltage control loop mainly influences the subsynchronous frequency, while the PLL affects the above and near the synchronous frequency [38, 39]. This paper will focus on the medium frequency, where the current control loop dominates.

To achieve zero error tracking at harmonic frequencies, Quasi-PR compensator with multi resonant frequencies can be applied, as $G_c(s)$ in Fig. 2 (a) and it is defined as

$$G_c(s) = K_p + \sum_{h=5,7,11,13\cdots} \frac{\frac{2K_{rh}h\omega_g}{Q}s}{s^2 + \frac{2h\omega_g}{Q}s + h^2\omega_g^2} \tag{1}$$

where $\omega_g=2\pi f_g$ is the fundamental angular frequency, K_p is proportional gain and K_{rh} is the gain at harmonic order h, Q is the quality factor. The time delay of the control loop is defined as

$$G_d(s) = e^{-1.5T_s s} \tag{2}$$

where T_s is the sampling period, and symmetrical sampling is applied. The output *LCL* filter has two critical frequencies, f_{r1} and f_{r2}, defined as

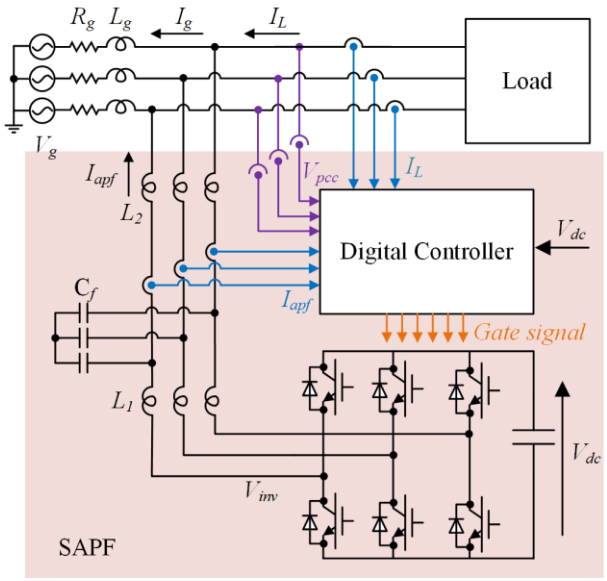

Fig. 1. A shunt active power filter together with load and grid.

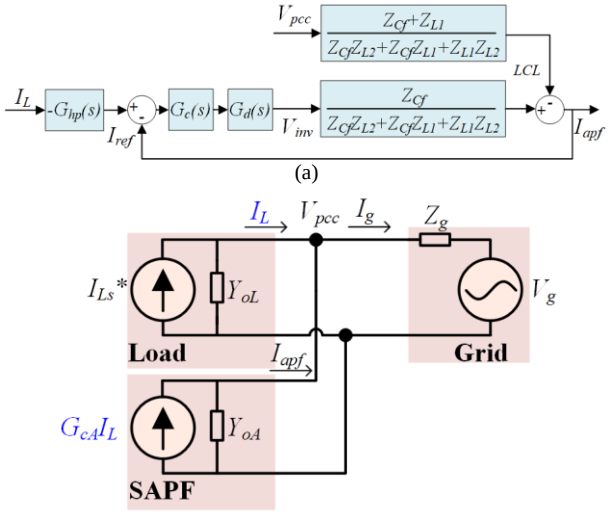

Fig. 2. (a) control diagram of SAPF, (b) equivalent circuit of the system.

$$f_{r1} = \frac{1}{2\pi\sqrt{L_1 C_f}} \tag{3}$$

$$f_{r2} = \frac{1}{2\pi}\sqrt{\frac{L_1 + L_2}{L_2 L_1 C_f}} \tag{4}$$

The close loop gains $G_{cA}(s)$ and output admittance $Y_{oA}(s)$ of SAPF can be easily derived from the control diagram in Fig.2, and they are

$$G_{cA}(s) = \frac{-G_{hp}(s)T_a(s)}{1+T_a(s)} \tag{5}$$

$$Y_{oA}(s) = \frac{Y_a(s)}{1+T_a(s)} = \frac{1}{\frac{1}{Y_a(s)} + \frac{T_a(s)}{Y_a(s)}} \tag{6}$$

where

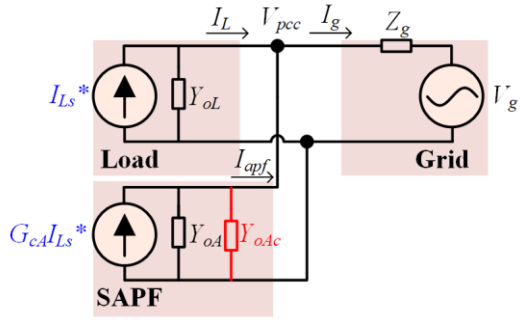

Fig. 3. Proposed impedance model of SAPF (with coupling admittance from the load) and the whole system.

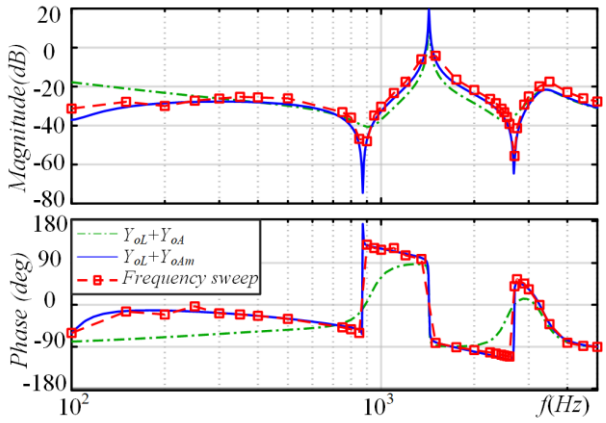

Fig. 4. Analytical admittance and frequency sweep results.

$$T_a(s)=\frac{G_c(s)G_d(s)Z_{Cf}}{Z_{L1}Z_{L2}+Z_{L1}Z_{Cf}+Z_{L2}Z_{Cf}} \tag{7}$$

$$Y_a(s)=\frac{Z_{Cf}+Z_{L1}}{Z_{L1}Z_{L2}+Z_{L1}Z_{Cf}+Z_{L2}Z_{Cf}} \tag{8}$$

Z_{L1}, Z_{L2} and Z_{Cf} are the impedance of L_1, L_2 and C_f branches in SAPF filter, respectively.

The system in Fig. 1 is then indicated as an impedance model, as shown in Fig. 2(b). Besides the output admittance of SAPF, the output admittance of the load Y_{oL} is also considered. As seen, the current source in the SAPF model is dependent on the load current, while the load current I_L can be depicted as,

$$I_L=I_{Ls}^{*}-Y_{oL}(s)V_{PCC} \tag{9}$$

where I_{Ls}^{*} is equivalent current source of load according to Norton principle. The current source in SAPF model then becomes

$$G_{CA}(s)I_L=G_{CA}(s)I_{Ls}^{*}-G_{CA}(s)Y_{oL}(s)V_{PCC} \tag{10}$$

whose second item is also an admittance. Therefore, the output admittance of the SAPF turns out to be

$$Y_{oAm}(s)=Y_{oA}(s)+Y_{oAc}(s)=Y_{oA}(s)-G_{cA}(s)Y_{oL}(s) \tag{11}$$

This extra item $Y_{oAc}(s)$ reflects the coupling between SAPF and load, and it also influences system stability. Meanwhile, the impedance model of SAPF and the system are modified from Fig. 2(b) to Fig. (3). According to the impedance stability criteria [32], the system stability is determined by $T(s)$ defined as

$$T(s)=Z_g(s)[Y_{oAm}(s)+Y_{oL}(s)] \tag{12}$$

B. Frequency sweep

To further verify the accuracy of the proposed model, a frequency-sweep of the SAPF and load output admittance is carried out. Due to the coupling between load and SAPF, output admittances of them are considered as a whole instead of individually. The parameters for load and SAPF in Case I in Table II are used, and the Grid impedance Z_g is set to be zero. A small perturbation is injected into the grid voltage V_g. Then, the total equivalent output admittance of SAPF and load can be calculated as a ratio between the grid voltage and current perturbation.

Fig.4 shows the admittance obtained from frequency sweep and the proposed admittance, which match each other very well. To indicate the impact of the coupling admittance, another admittance w/o the coupling admittance is also shown as the dashed curve. A significant error between it and the frequency sweep result is observed.

III. Stability Region

Based on the proposed model, system stability can be easily analyzed if the load admittance and grid impedance are both known. Yet, in reality, the impedance of a distributed system is time-variant and thereby is challenging to measure accurately. The load admittance is not easy to measure precisely, neither. Therefore, in this section, the passivity region and stability region for load admittance are explored, where a specific and precise load admittance is not necessary for stability analysis.

A. Passivity criterion

As known, the grid is usually considered to be intrinsically passive. Thus, according to the passivity criteria [40], the stability of the system is determined by load and SAPF. As long as the summation of these two output admittance is passive, the system is stable. To be passive, the total output admittance $Y_{total}(s)$ must meet two requirements as follows,

- $Y_{total}(s)$ has no Right-Half-Plane (RHP) pole
- $\mathrm{Re}\{Y_{total}(j\omega)\}\geq 0 \Leftrightarrow \arg\{Y_{total}(j\omega)\}\in[-90^{\circ},90^{\circ}],\forall\omega>0$

According to [41], the paralleled or series-connection of several passive systems is still passive. From the impedance model of the system shown in Fig. 3, the total output admittance is easily obtained as (13), which consists of two parts. The first part, $Y_{oA}(s)$, is solely determined by SAPF itself. The second part, $-G_{cA}(s)Y_{oL}(s)+Y_{oL}(s)$, is affected by both load output admittance and SAPF design. The high pass filter $G_{hp}(s)$ in $G_{cA}(s)$ for the reference current extraction can be simplified to 1 above the fundamental frequency. Then substituting (5), and (6) into (13), (14) is obtained.

$$Y_{total}(s)=Y_{oA}(s)-G_{cA}(s)Y_{oL}(s)+Y_{oL}(s) \tag{13}$$

$$Y_{total}(s)=Y_{oA}(s)+\frac{1}{1+T_a(s)}Y_{oL}(s)=\frac{Y_a(s)+Y_{oL}(s)}{1+T_a(s)} \tag{14}$$

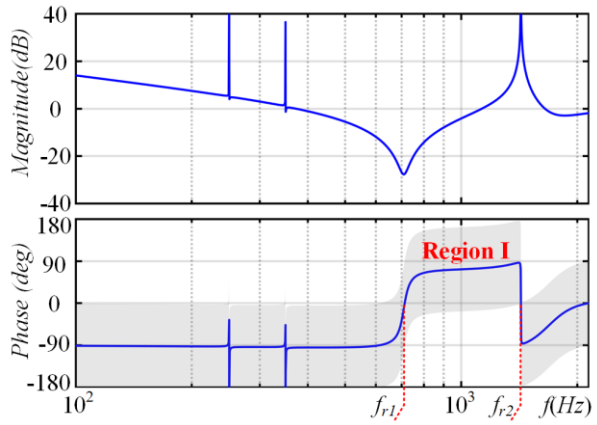

Fig. 5. Bode plot of $1+T_a(s)$

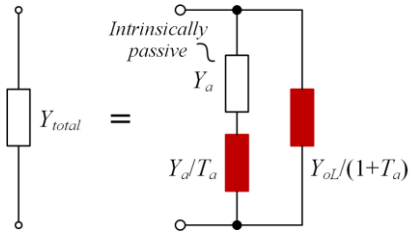

Fig. 6. Decomposition of Y_{total}

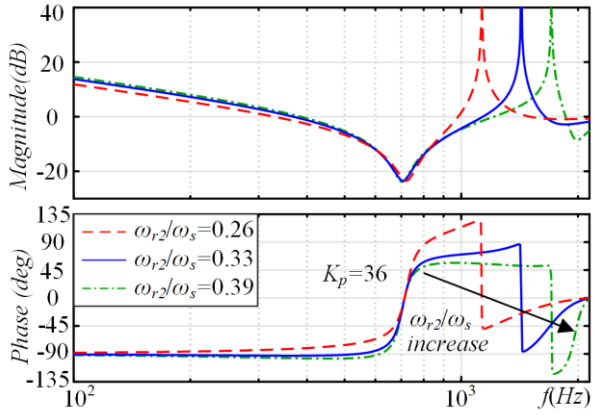

Fig. 7. Bode plot of $1+T_a(s)$ with different ω_{r2}/ω_{r1}

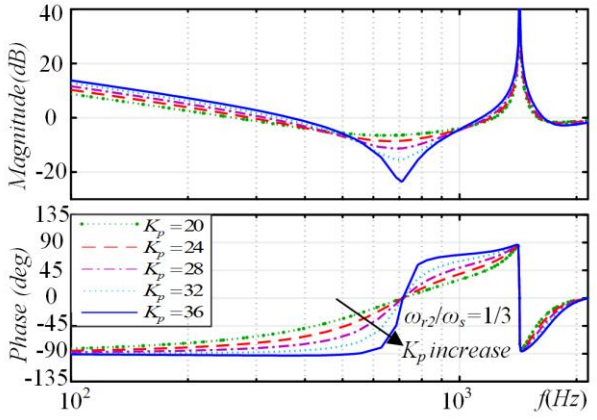

Fig. 8. Bode plot of $1+T_a(s)$ with different K_p

For $Y_{total}(s)$, its denominator,$1+T_a(s)$, is determined by SAPF and should have no RHP zero, otherwise, SAPF itself will be unstable no matter what the grid or load condition is. When the phase difference between $Y_a(j\omega)+Y_{oL}(j\omega)$ and $1+T_a(j\omega)$ is less than 90 degrees, the real part of $Y_{total}(s)$ will be positive and thereby $[Y_a(s)+Y_{oL}(s)]/[1+T_a(s)]$ is passive. That is to say, the phase of $Y_a(s)+Y_{oL}(s)$ should locate in the shadow region (Region I) illustrated in Fig.5. The Region I is flexible and it can be adjusted to fit $Y_a(s)+Y_{oL}(s)$ by changing parameters of SAPF, such as resonant frequencies f_{r1} and f_{r2} of its *LCL* filter, sampling frequency f_s, proportional gain K_p, etc. More explanation is as follows.

B. Passivity region

According to (14), $Y_{total}(s)$ can be decomposed into three admittances, as shown in Fig.6. $Y_{total}(s)$ will be passive if these three admittances are individually passive. $Y_a(s)$, as illustrated in (8), is intrinsically passive because it is a network composed of RLC components. The other two items have the open-loop transfer function $T_a(s)$ involved, thus might be active and need further analysis as follows. According to (3), (7) and (8), it can be obtained,

$$\frac{Y_a(s)}{T_a(s)}=\frac{Z_{Cf}+Z_{L1}}{G_c(s)G_d(s)Z_{Cf}}=\frac{L_1C_f(\omega_{r1}^2+s^2)}{G_c(s)G_d(s)} \tag{15}$$

Due to the resonant item of the compensator $G_c(s)$, $|1+T_a| >>1$ at resonant frequencies. Therefore according to (12) and (14), the open loop transfer function which determines the stability of the system $|T(s)|<<1$ at resonant frequencies. It means the Nyquist curve of T(s) will not cross -180 degree from the left side of (-1,0) at the resonant frequencies. Meanwhile the resonant part of $G_c(s)$ influences only near the resonant frequencies as long as the quality factor Q is high. Thus the resonant part in $G_c(s)$ will not influence the system stability. The resonant part can still affect the loop gain of the APF and lead to instability. However, as the issue has been studied a lot in literature, it is not discussed here. The analysis in this paper is based on assumption that the loop gain of the APF has no stability issue with a proper design. Therefore, only the proportional gain K_p of the compensator is considered for simplicity. It is then obtained,

$$\frac{Y_a(j\omega)}{T_a(j\omega)}=\frac{L_1C_f(\omega_{r1}^2-\omega^2)[\cos(1.5\omega T_s)+j\sin(1.5\omega T_s)]}{K_p} \tag{16}$$

When the resonant frequency f_{r1} is equal to 1/6 of sampling frequency f_s, the real part of (16) will never be negative within the Nyquist frequency range and therefore $Y_a(s)/T_a(s)$ is passive.

As for the last term $Y_{oL}(s)/[1+T_a(s)]$, $Y_{oL}(s)$is independent from $1+T_a(s)$. Hence, it can be passive when the phase difference between $Y_{oL}(s)$ and $1+T_a(s)$ is in $[-90^o, 90^o]$, which is exactly the Region I in Fig.5. Therefore, Region I is also called the passivity region and can be changed to fit the load output admittance $Y_{oL}(s)$.

For those loads that is capacitive in only one frequency range, f_{r1} and f_{r2} should be set at the lower and upper limit of this frequency range, respectively. Meanwhile, the sampling frequency f_s is always set to be 6 f_{r1}. The passivity region around the resonant frequencies of $G_c(s)$ might be narrow and thereby difficult to cover $Y_{oL}(s)$, however as mentioned above, the resonant item in $G_c(s)$ will not influence the stability of the system. More flexibility of the passivity region is discussed as follows.

As shown in Fig.7, the phase angle for $1+T_a(s)$ near f_{r2} varies with the ratio of frequency f_{r2} and f_s. In this way, it can be

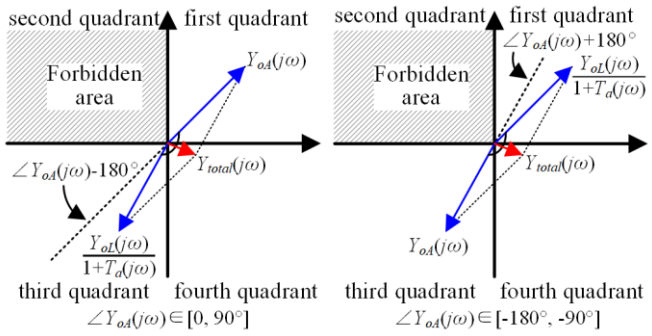

Fig. 9. Phasor diagram of $[Y_a(s)+Y_{oL}(s)]/[1+T_a(s)]$

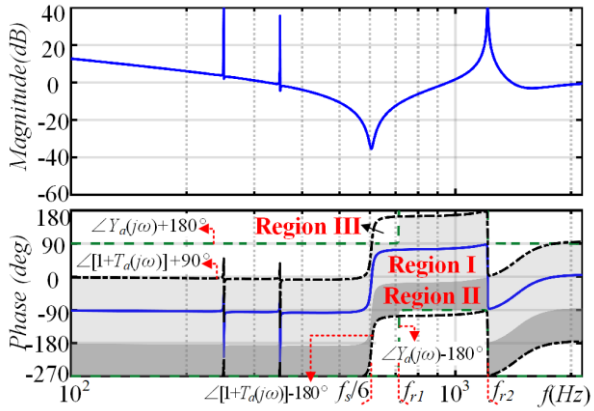

Fig. 10. Bode plot of $1+T_a(s)$ with an expanded region

adjusted to fit the loads. $1+T_a(s)$ near f_{r2} can be calculated as follows according to (7),

$$1+T_a(j\omega)\big|_{\omega\to\omega_{r2}} = 1+\frac{K_P e^{-1.5j\omega_{r2}T_s}}{L_1L_2C_f\, j\omega(-\omega^2+\omega_{r2}^2)}\bigg|_{\omega\to\omega_{r2}} \tag{17}$$

whose phase angle is then obtained as,

$$\angle\left[1+T_a(j\omega)\big|_{\omega\to\omega_{r2}}\right] = \begin{cases} \frac{\pi}{2}\left(-\frac{6\omega_{r2}}{\omega_s}+3\right), if\ \omega<\omega_{r2} \\ \frac{\pi}{2}\left(-\frac{6\omega_{r2}}{\omega_s}+1\right), if\ \omega>\omega_{r2} \end{cases} \tag{18}$$

As seen, if the ratio of f_{r2} and f_s is 1/3, the phase jump from 90° to -90° at f_{r2}, which makes the passivity region easier to cover $Y_{oL}(s)$.

In addition, the proportional gain K_p, mainly related to the phase change per frequency, as shown in Fig.8, can be lower to smooth the phase near f_{r1}. Moreover, active or passive damping can be applied to restrain the dramatic phase jump near f_{r2}, leading to the connection of two parts of Region I.

C. Stability region

However, the passive criterion is hard to meet because of the strict requirements. The passive criterion is a sufficient but not necessary condition for stability. The stability region, which is less conservative and more practical, is then analyzed as follows.

According to (12) and (14), $T_m(s)$ that determines the stability of the system becomes,

$$T_m(s) = Z_g(s)Y_{total}(s) = \frac{Z_g(s)[Y_a(s)+Y_{oL}(s)]}{1+T_a(s)} \tag{19}$$

The system will be stable, as long as the phase of $T_m(s)$ stays in [-180°, 180°]. According to (19), $T_m(s)$ is comprised of $Y_{total}(s)$ and $Z_g(s)$ and their phase relationship is as follow,

$$\angle T_m(j\omega) = \angle Z_g(j\omega)+\angle Y_{total}(j\omega) \tag{20}$$

In most of the scenarios, the grid impedance $Z_g(s)$ is inductive and thus its phase is between 0 and 90°. Then, to ensure that $\angle T_m(j\omega)$ is within the required range for any inductive grid impedance, the allowed phase range for $Y_{total}(j\omega)$ is [-180°, 90°].

To depict the stability region for load admittance solely, the total output admittance $Y_{total}(s)$ is decomposed into two parts, $Y_{oA}(s)$ and $Y_{oL}(s)/[1+T_a(s)]$, conforming to (14). Even the phase of both parts is in [-180°, 90°], is not a sufficient condition because the sum of two vectors, one in the first quadrant and another in the third quadrant, is possible to be in the second quadrant. More details are discussed as follows.

For the first item $Y_{oA}(s)$, if the switching frequency f_s is set to $6f_{r1}$, $Y_{oA}(s)$ is passive according to the analysis in Section III-B. But it is difficult to realize due to the parameter variation of LCL elements. In light of (3), (4), (7) and (8), $Y_a(j\omega)$ and $1+T_a(j\omega)$ can be written as

$$Y_a(j\omega) = j\frac{(\omega^2-\omega_{r1}^2)}{L_2\omega(\omega_{r2}^2-\omega^2)} \tag{21}$$

$$1+T_a(j\omega) = 1-\frac{K_p\sin(1.5\omega T_s)}{L_1L_2C_f\omega(\omega_{r2}^2-\omega^2)} - \frac{jK_p\cos(1.5\omega T_s)}{L_1L_2C_f\omega(\omega_{r2}^2-\omega^2)} \tag{22}$$

First of all, to accurately control the grid current, SAPF will apply a grid current feedback control. Therefore, $f_{r2} > f_s/6$ should be ensured to make the SAPF stable itself.

a) $f_{r1} < f_s/6$. The phase of $Y_a(j\omega)$ in the range $[f_{r1}, f_s/6]$ is 90°, while $1+T_a(j\omega)$ is in the fourth quadrant where its phase is smaller than zero. Thus, $Y_{oA}(j\omega)$ will be in the second quadrant.

b) $f_s/6 < f_{r1}$. The phase of $Y_a(j\omega)$ is the range $[f_s/6, f_{r1}]$ is -90°, while $1+T_a(j\omega)$ is in the first quadrant. Thus, $Y_{oA}(j\omega)$ will be in the third quadrant. Similarly, in the range $[0, f_s/6]$, $Y_{oA}(j\omega)$ will be in the fourth quadrant, in the range $[f_{r1}, f_s/2]$, $Y_{oA}(j\omega)$ will be in the first quadrant.

Consequently, $f_s/6 \leqslant f_{r1}$ will be a necessary condition.

For $Y_{oA}(j\omega)$ locating in the first quadrant, the phase of $Y_{oL}(j\omega)/[1+T_a(j\omega)]$ should be within $[\angle Y_{oA}(j\omega)$ -180°, 90°] as illustrated in Fig.9 (a). Otherwise, $Y_{total}(j\omega)$ will easily enter the forbidden region when the magnitude of $Y_{oL}(j\omega)/[1+T_a(j\omega)]$ is large. Similarly, for $Y_{oA}(j\omega)$ locating in the third quadrant, the phase of $Y_{oL}(j\omega)/[1+T_a(j\omega)]$ should be within [-180°, $\angle Y_{oA}(j\omega)$+180°] as depicted in Fig.9 (b).

For $Y_{oA}(j\omega)$ locates in the fourth quadrant, then as long as $Y_{oL}(j\omega)/[1+T_a(j\omega)]$ is not in the second quadrant, $Y_{total}(j\omega)$ will never enter the forbidden region.

From the analysis above, the limitation of $Y_{oL}(j\omega)$ phase then can be derived as (23).

$$\begin{aligned}\angle Y_{oL}(j\omega) \in &\left[\angle Y_a(j\omega)-180^o, \angle Y_a(j\omega)+180^o\right] \\ \cap &\left[\angle[1+T_a(j\omega)]-180^o, \angle[1+T_a(j\omega)]+90^o\right]\end{aligned} \tag{23}$$

Then, the region expands from Region I to Region I + Region II – Region III as depicted in Fig.10, namely stability region. If the switching frequency f_s is equal to $6f_{r1}$, Region III will be zero. Moreover, the stability region is continuous at f_{r2}, which is however not the case for the passivity region.

TABLE I. COMPARISON OF PASSIVITY AND STABILITY REGION.

Method	Grid impedance	Stable region	Switching frequency	continuity
passivity region	Any impedance	Region I	$f_s = 6f_{r1}$	Discontinuous at f_{r2}
Stability region	Inductive	Region I +Region II- Region III	$f_s \leqslant 6f_{r1}$	Continuous at all frequency

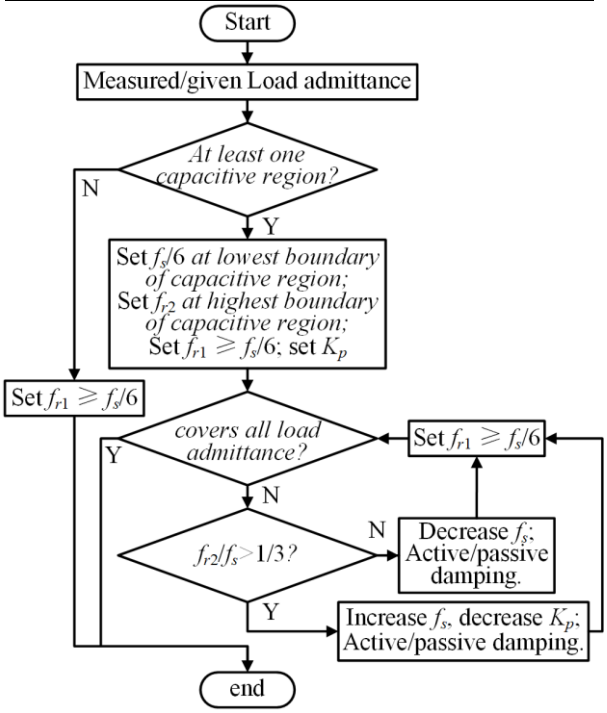

Fig. 11. Stability-oriented design of SAPF

D. Stability-oriented design

A comparison of these two methods is elaborated in Table I. As mentioned above, the grid impedance is mostly inductive, thus the stability region is easier to achieve because: 1. The stability region covers most of the passivity region and is beyond it，making it suitable for multi-capacitive region load; 2. The switching frequency f_s does not need to be equal to 6 f_{r1}; 3. The passivity region jumps at f_{r2}, while the stability region is continuous at any frequency.

A flow chart shown in Fig. 11 summarizes the stability-oriented design of SAPF based on the analysis above. First, the load admittance might be given or measured, which could be a specific curve or a region. If no capacitive region exists, the resonance frequency f_{r1} and f_{r2} can be designed according to other requirements and the switching frequency $f_{r1} \geqslant f_s/6$. Otherwise, set $f_s/6$ as the lowest boundary of the capacitive region and f_{r2} as the highest boundary of the capacitive region. K_p is determined by the current loop. After that, if the stability region does not cover load admittance at all frequencies, parameters should be adjusted to fit the phase of load admittance until the stability region covers load admittance at all frequencies.

When the frequency ratio f_{r2}/f_s is larger than 1/3, the uncovered region appears above f_{r2} because the phase of $1+T_a(j\omega)$ might be smaller than -90° at this frequency range. Thus, the inductive region is not fully covered by the stability region. Switching frequency f_s can be increased to change the frequency ratio and proportional gain K_p can be decreased if the phase change of load at $f_s/6$ is slow. Moreover, active or passive damping should be adopted to suppress the phase jump. When the frequency ratio f_{r2}/f_s is smaller than 1/3, the uncovered region appears at frequency smaller than f_{r2} because the phase of $1+T_a(j\omega)$ might be larger than 90 degrees at this frequency range. Therefore, decreasing the switching frequency or adding damping at f_{r2} can adjust the stability region to cover the load admittance.

IV. EXPERIMENTAL VALIDATION

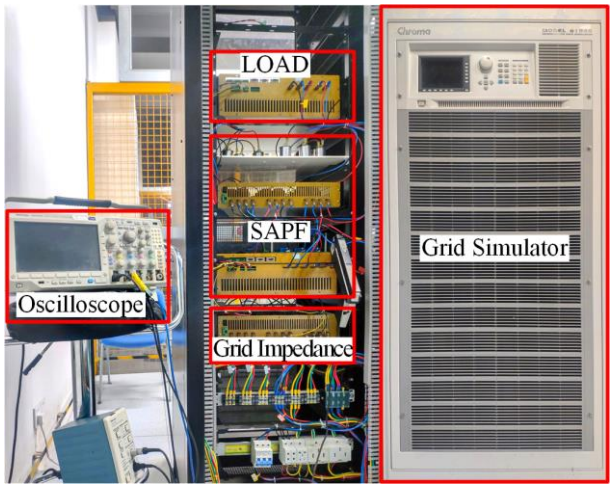

Fig. 12. A test platform.

TABLE II. PARAMETERS USED IN EXPERIMENTS

		Symbol	Meaning	Value
Base Case II	Grid	V_s	Grid voltage	190 V
		L_g	grid inductor	1.6 mH
		f_g	Grid frequency	50 Hz
	SAPF	V_{dc}	DC-link voltage	400 V
		f_s	Switching frequency	4.28 kHz
		K_p	Proportional gain	18
		L_1	Converter side filter inductor	9.45 mH
		C_f	Filter Capacitor	5.26 uF
		L_2	Grid side filter inductor	3.15 mH
	Load	L_{1L}	Converter side filter inductor	9.45 mH
		L_{2L}	Grid side filter inductor	3.15 mH
		C_{fL}	Filter Capacitor	5.26 uF
		I_{Lrms}	Load current (RMS)	3.6 A
		h	Harmonic order	5^{th} , 7^{th}
Modification Case I		C_f	Filter Capacitor (SAPF)	1 uF
		K_p	Proportional gain	39
		f_s	Sampling frequency	10 kHz
Modification Case III		L_g	Grid inductor	3.2 mH
Modification Case IV		I_{Lrms}	Load current (RMS)	6 A
Modification Case V		f_s	Switching frequency	4.10 kHz
		C_{fL}	Filter Capacitor(load)	0 uF

To verify the above analysis, the system depicted in Fig.1 is established, and it is shown in Fig. 12. A Chroma 61800-series

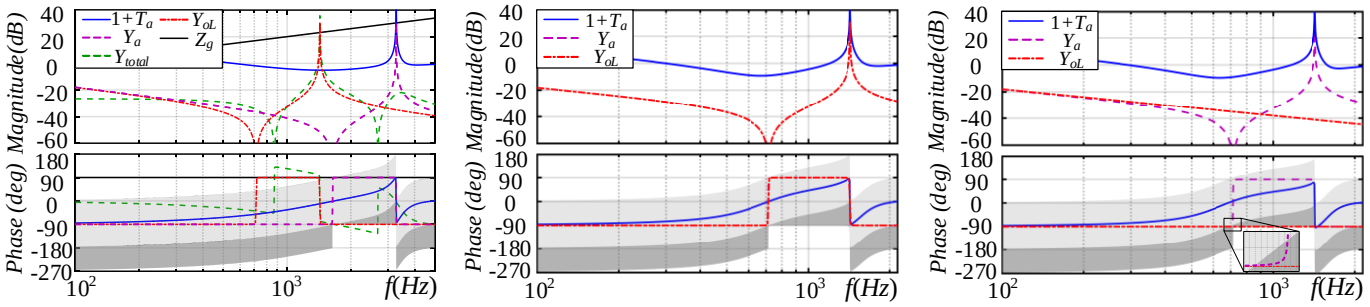

(a)Case I (b) Case II~IV (c) Case V

Fig. 13. Bode plot of Ya, YoL and 1+Ta for case I~V

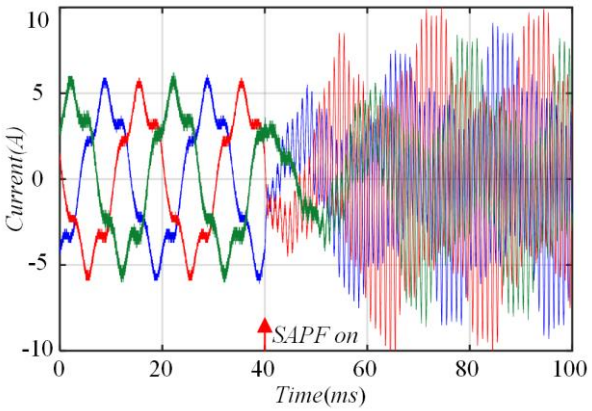

Fig. 14. Experimental grid current with parameters in Case I

ac power supply is used for emulating the grid. The grid impedance is inductive. A three-phase rectifier with open loop control and pulse width modulation in series with LCL filter is used to imitate a passive load, which behaves capacitive in a frequency range. The parameters of the test are listed in Table II.

As seen, five cases with different configurations of the system are tested. Case II is the base case. On top of it, the SAPF output admittance has a significant change in Case I; only the grid inductance changes in Case III; the load current is doubled in Case IV; the filter of load changes from *LCL* to *L* and the switching frequency is reduced in Case V.

Bode plot of Y_a, Y_{oL} and 1+T_a, and the stability region are shown in Fig. 13. The phase of Y_a locates in the light shadow region (Region I) in Case I~IV. Therefore, if the load dynamic is ignored, the output admittance of SAPF $Y_a(s)/[1+T_a(s)]$ is passive. It means that these cases should be stable according to passivity criteria. However, the experimental result in Fig. 14 shows Case I loses stability once the SAPF is kicked in, which proves that the load dynamic in output admittance of SAPF cannot be ignored for stability analysis. The instability is also reflected by the bode plot in Fig. 13 (a), where $Y_{oL}(s)$ is out of the stability region.

In Case II, Y_{oL} is in the passivity region (region I), and the system is indeed stable after SAPF is kicked in, as shown in Fig. 15(a). On top of it, the grid inductance is doubled in Case III, and the load current is doubled in Case IV; however, they do not change the admittance of load or SAPF (seen Fig. 13 (b)), thus, the system is still stable (see Fig. 15 (b) and (d)). In Case V, the filter of the load is changed from *LCL* to *L*, and thereby the load admittance Y_{oL} changes, which is not covered by passivity region (region I) but stability region (region I + region II - region III), as seen in Fig. 13 (c). In the end, the system is still stable (see Fig. 15 (c)), which again validates the stability region. It should be noted that $f_{r1} = f_s/6$ in Case II~IV, which is a condition of passivity region. Meanwhile the load admittance Y_{oL} indeed locates in the passivity region and the system is stable. In Case V, the switching frequency f_s is reduced, so $f_{r1} > f_s/6$. However, since the load admittance Y_{oL} is still in stability region, the system is still stable. As a result, both passivity and stability regions are validated. Further, $f_{r2}/f_s = 1/3$ in Case II~IV, but f_{r2}/f_s is slightly larger than 1/3 in Case V. It proves that $f_{r2}/f_s = 1/3$ is not a strict condition for stability.

Additionally, the spectrums of grid currents are shown before and after the SAPF kicks in, as seen in Fig. 15 (a)~(c). The grid current harmonics are mainly at 5th and 7th. After the SAPF kicks in, the harmonics are significantly mitigated. A load change, which is essentially a transition from Case II to IV, is also demonstrated in Fig. 15 (d). As seen, the stability of the system is ensured during the transition. The dc side voltage of SAPF does not have significant dip, because SAPF only generates harmonic current, and the fundamental current is only used to compensate the power loss in the components. Thus there is no dramatic active power change in SAPF during load step

V. Conclusion

In this paper, an accurate admittance model for SAPF is developed. The coupling between SAPF and load is revealed, which shows a significant impact on the model. More importantly, based on the developed admittance model of SAPF, the stability region of the system is investigated. The passivity region of the load admittance to guarantee the system stability is firstly explored. However, the passivity region has rigorous boundary conditions, which are difficult to achieve in reality. The stability region is then studied, and it turns out to have much less strict boundary conditions, thereby much easier to fulfill. The stability region defined in this paper provides a guide to SAPF for valid application scenarios, where an accurate admittance model of the load is not required. Instead, more general knowledge of the admittance model (capacitive, inductive, or resistive) is sufficient to judge the stability of the system. The stability-oriented design is then summarized in a flow chart. In the end, the effectiveness of the newly defined stability region is verified by experimental results.

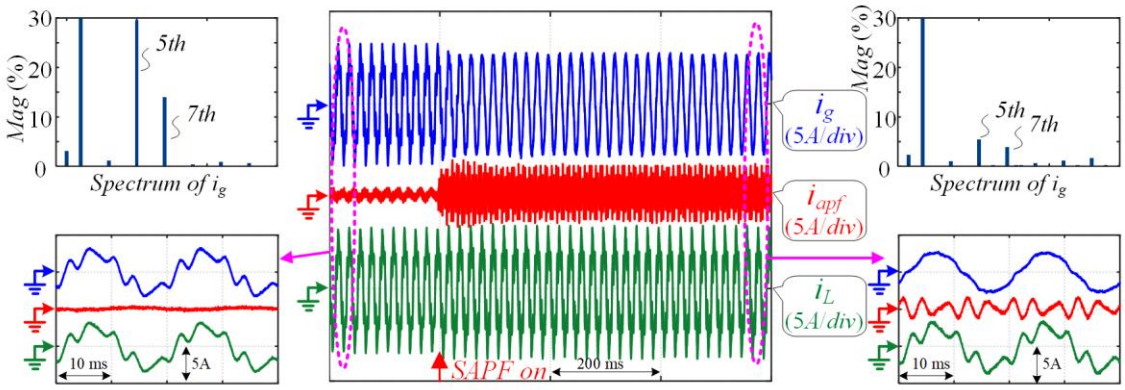

(a) Case II (base case)

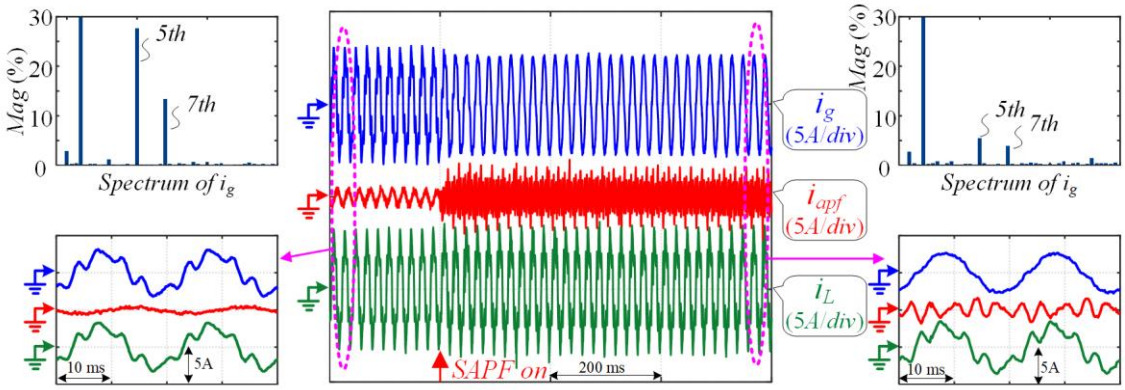

(b) Case III (grid inductance is doubled)

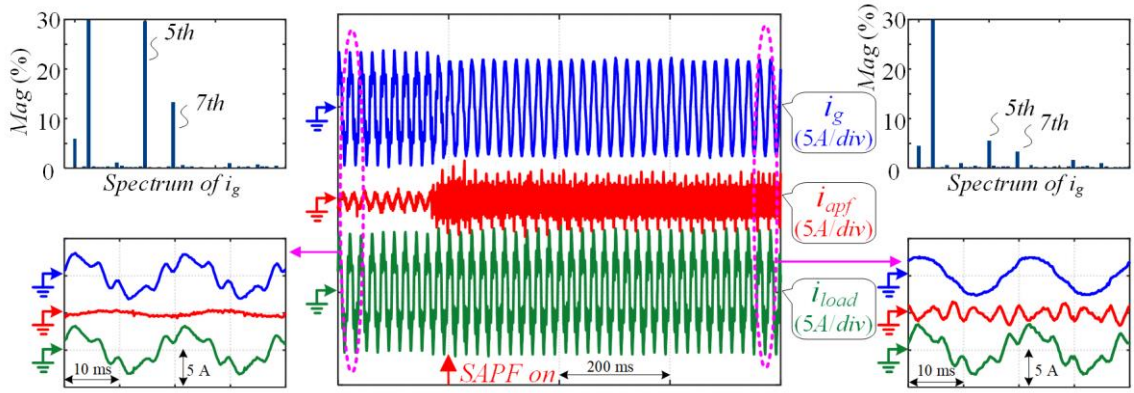

(c) Case V (load admittance becomes pure inductive)

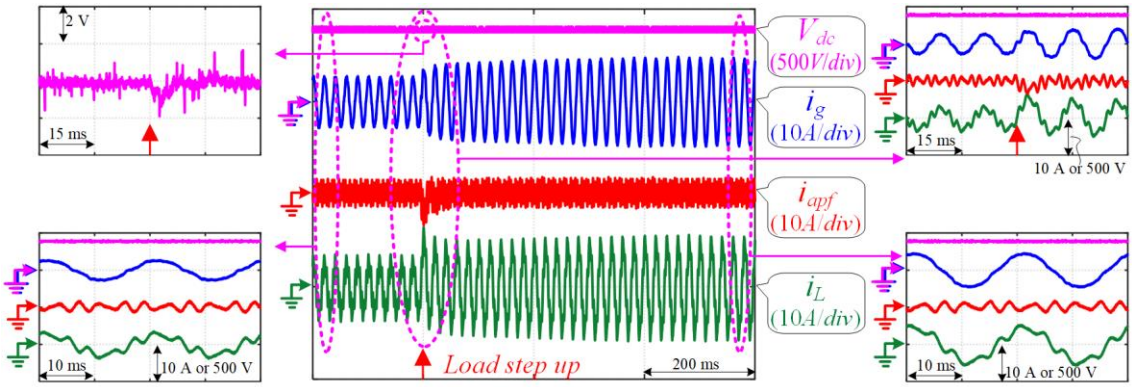

(d) load change (from case II to case IV)

Fig. 15. Experimental results with SAPF kick in and load step to verify the stability region.

REFERENCES

[1] Y.P. Siwakoti, F. Peng, F Blaabjerg, P.C. Loh, G.E. Town, "Impedance-Source Networks for Electric Power Conversion Part I: A Topological Review," *IEEE Transactions on Power Electronics*, vol. 30, no. 2, pp. 699-716, Mar 2014.

[2] T. Dragičević, X. Lu, J. Vasquez, J. Guerrero, " DC Microgrids—Part II: A Review of Power Architectures, Applications, and Standardization Issues," *IEEE Transactions on Power Electronics*, vol. 31, no. 5, pp. 3528-3549, Aug 2015.

[3] G. Zhang, J. Chen, B. Zhang, and Y. Zhang, "A Critical Topology Review of Power Electronic Transformers: In View of Efficiency," *Chinese Journal of Electrical Engineering*, vol. 4, no. 2, pp. 90-95, Jun 2018.

[4] C. Li, Q. Guan, J. Lei, C. Li, Y. Zhang, S. Wang, D. Xu, W. Li, and H. Ma, "An SiC MOSFET and Si Diode Hybrid Three-Phase High-Power Three-Level Rectifier," *IEEE Transactions on Power Electronics*, vol. 34, no. 7, pp. 6076-6087, Jul 2019.

[5] H. Soltani, P. Davari, F. Zare, and F. Blaabjerg, "Effects of Modulation Techniques on the Input Current Interharmonics of Adjustable Speed Drives," *IEEE Transactions on Industrial Electronics*, vol. 65, no. 1, pp. 167-178, Jan 2018.

[6] Y. Yang, P. Davari, F. Zare, and F. Blaabjerg, "Enhanced Phase-Shifted Current Control for Harmonic Cancellation in Three-Phase Multiple Adjustable Speed Drive Systems," *IEEE Transactions on Power Delivery*, vol. 32, no. 2, pp. 996-1004, Apr 2017.

[7] F. Masaaki and S. Hiroshi, "An Analytical Method for Calculating Harmonic Currents of a Three-phase Diode-Bridge Rectifier with dc Filter," *IEEE Transactions on Power Electronics*, vol. 9, no. 6, pp. 631-637, Nov 1994.

[8] L. Beloqui Larumbe, Z Qin, P Bauer, "Introduction to the analysis of harmonics and resonances in large offshore wind power plants," in *2018 IEEE International Power Electronics and Motion Control Conference (PEMC)*, Budapest, Hungary, 2018, pp. 393-400.

[9] C. Chou, C. Liu, J. Lee, and K. Lee, "Optimal planning of large passive-harmonic-filters set at high voltage level," *IEEE Transactions on Power Systems*, vol. 15, no. 1, pp. 433-441, Feb 2000.

[10] C. Kawann and A. E. Emanuel, "Passive shunt harmonic filters for low and medium voltage: a cost comparison study," *IEEE Transactions on Power Systems*, vol. 11, no. 4, pp. 1825-1831, Nov 1996.

[11] S. S. Patil, R. A. Metri and O. K. Shinde, "Shunt active power filter for MV 12-pulse rectifier using PI with SMC controller," in *2017 International Conference on circuits Power and Computing Technologies (ICCPCT)*, Kollam, India, 2017, pp. 1-6.

[12] S. Rahmani, K. Al-Haddad and F. Fnaiech, "A Three-Phase Shunt Active Power Filter for Damping of Harmonic Propagation in Power Distribution Systems," in *2006 IEEE International Symposium on Industrial Electronics (ISIE)*, Montreal, Quebec, Canada, 2006, pp. 1760-1764.

[13] X. Chen, K. Dai, C. Xu, L. Peng, and Y. Zhang, "Harmonic compensation and resonance damping for SAPF with selective closed-loop regulation of terminal voltage," *IET Power Electronics*, vol. 10, no. 6, pp. 619-629, Apr 2017.

[14] C. Xu, K. Dai, X. Chen, L. Peng, Y. Zhang, and Z. Dai, "Parallel Resonance Detection and Selective Compensation Control for SAPF With Square-Wave Current Active Injection," *IEEE Transactions on Industrial Electronics*, vol. 64, no. 10, pp. 8066-8078, Oct 2017.

[15] M. Suresh, S. S. Patnaik, Y. Suresh, and A. K. Panda, "Comparison of two compensation control strategies for shunt active power filter in three phase four-wire system," in *2011 Innovative Smart Grid Technologies (ISGT)*, Anaheim, CA, USA, 2011, pp. 1-6.

[16] B. L. G. Costa, V. D. Bacon, S. A. O. Da Silva, and B. A. Angelico, "Tuning of a PI-MR Controller Based on Differential Evolution Metaheuristic Applied to the Current Control Loop of a Shunt-APF," *IEEE Transactions on Industrial Electronics*, vol. 64, no. 6, pp. 4751-4761, Jun 2017.

[17] K. Dai, C. Liu, K. Duan, and Y. Kang, "Harmonic compensation characteristics of active power filters to nonlinear loads based on impedance analysis," in *2012 IEEE International Symposium on Industrial Electronics*, Hangzhou, China, 2012, pp. 340-347.

[18] X. Mu, J. Wang, W. Wu, and F. Blaabjerg, "A Modified Multifrequency Passivity-Based Control for Shunt Active Power Filter With Model-Parameter-Adaptive Capability," *IEEE Transactions on Industrial Electronics*, vol. 65, no. 1, pp. 760-769, Jan 2018.

[19] W. Cao, K. Liu, M. Wu, S. Xu, and J. Zhao, "An Improved Current Control Strategy Based on Particle Swarm Optimization and Steady-State Error Correction for SAPF," *IEEE Transactions on Industry Applications*, vol. 55, no. 4, pp. 4268-4274, Jul 2019.

[20] S. Ouchen, M. Benbouzid, F. Blaabjerg, A. Betka, and H. Steinhart, "Direct Power Control of Shunt Active Power Filter using Space Vector Modulation based on Super Twisting Sliding Mode Control," *IEEE Journal of Emerging and Selected Topics in Power Electronics*, Early Access, 2020.

[21] Z. Hao, Z. Fang, C. Zhu, H. Yi, Z. Wang, R. Tan, and T. Wei, "An Optimal Compensation Method of Shunt Active Power Filters for System-Wide Voltage Quality Improvement," *IEEE Transactions on Industrial Electronics*, vol. 67, no. 2, pp. 1270-1281, Feb 2020.

[22] K. Liu, W. Cao, and J. Zhao, "Dual-Loop-Based Harmonic Current Control Strategy and Admittance Modeling for a Multimodular Parallel SAPFs System," *IEEE Transactions on Industrial Electronics*, vol. 67, no. 7, pp. 5456-5466, Jul 2020.

[23] Q. Liu, Y. Li, S. Hu, and L. Luo, "Power quality improvement using controllable inductive power filtering method for industrial DC supply system," *Control Engineering Practice*, vol. 83, pp. 1-10, Feb 2019.

[24] Q. Liu, Y. Li, S. Hu, and L. Luo, "A transformer integrated filtering system for power quality improvement of industrial DC supply system," *IEEE Transactions on Industrial Electronics*, vol. 67, no. 5, pp. 3329-3339, May 2020.

[25] B. Rao, Y. Suresh, A. Panda, and B. Naik, "Development of cascaded multilevel inverter based active power filter with reduced transformers," *CPSS Transactions on Power Electronics and Applications*, vol. 5, no. 2, pp. 147-157, Jun 2020.

[26] C. Liu, K. Dai, X. Chen, Y. He, and P. Lu, "Selective Harmonic Suppression Strategy by SAPF in Power Distribution System," *The Journal of Engineering*, vol. 2017, no. 13, pp. 1-4, Oct 2017.

[27] A. Panchbhai, N. Prajapati and S. Parmar, "Comparative study of reference current generation for shunt active power filter," in *2017 International Conference on Power and Embedded Drive Control (ICPEDC)*, Chennai, India, 2017, pp. 381-386.

[28] S. Karvekar and D. Patil, "Comparison of reference current generation for shunt active power filter using Goertzel Algorithm and Enhanced PLL," in *2014 International Conference on Circuits, Power and Computing Technologies (ICCPCT)*, Nagercoil, India, 2014, pp. 620-625.

[29] Y. Bing, D. Jiang, Y. Liang, L. Yang, P. Qiu, and F. Xu, "Improved Modeling, Stability Analysis and Resonance Suppression of APF System," in *2018 IEEE International Power Electronics and Application Conference and Exposition (PEAC)*, Shenzhen, China, 2018, pp. 1-5.

[30] Y. Bing, D. Jiang, Y. Liang, C. Jiang, T. He, L. Yang, and P. Hu, "Modified Modeling and System Stabilization of Shunt Active Power Filter Compensating Loads with μF Capacitance," *Energies*, vol. 12, p. 1-19, May 2019.

[31] Y. JingRong, C. Meihong, D. Gao, G. Ying, and Y. Jiaqi, "A Lyapunov stability theory-based control method for three-level shunt active power filter," in *2016 Proceedings of the 35th Chinese Control Conference*, Chengdu, China, 2016, pp. 8683-8687.

[32] R. Middlebrook, "Input filter considerations in design and application of switching regulators," in Proc. IEEE IAS, 1976, pp. 366–382.

[33] J. Sun, "Impedance-Based Stability Criterion for Grid-Connected Inverters," *IEEE Transactions on Power Electronics*, vol. 26, no. 11, pp. 3075-3078, Nov 2011.

[34] L Beloqui Larumbe, Z Qin, P Bauer, "Output Impedance Modelling and Sensitivity Study of Grid-Feeding Inverters with Dual Current Control," in *2019 Annual Conference of the IEEE Industrial Electronics Society (IECON)*, Lisbon, Portugal, Portugal, 2019, pp. 4007-4012.

[35] J. Sun, "Small-signal methods for AC distributed power systems—A review," IEEE Trans. Power Electron., vol. 24, no. 11, pp. 2545–2554, Nov. 2009.

[36] X. Wang, F. Blaabjerg, " Harmonic Stability in Power Electronic-Based Power Systems: Concept, Modeling, and Analysis," IEEE Trans. Smart Grid, vol. 10. no. 3, pp. 2858-2870, 2019.

[37] J. Lei, Z. Qin, W. Li, P. Bauer, X. He, " Modelling of Output Admittance Coupling Between Shunt Active Power Filters and Non-linear Loads," in Proc. of IEEE-eGrid's 2019, 2019

[38] B. Wen, D. Boroyevich, R. Burgos, P. Mattavelli and Z. Shen, "Analysis of D-Q Small-Signal Impedance of Grid-Tied Inverters," in IEEE Transactions on Power Electronics, vol. 31, no. 1, pp. 675-687, Jan. 2016.

[39] X. Wang, L. Harnefors and F. Blaabjerg, "Unified Impedance Model of Grid-Connected Voltage-Source Converters," in IEEE Transactions on Power Electronics, vol. 33, no. 2, pp. 1775-1787, Feb. 2018.

[40] Z. Zhang, W. Wu, Z. Shuai, X. Wang, A. Luo, H. S. Chung, and F. Blaabjerg, "Principle and Robust Impedance-Based Design of Grid-tied Inverter with *LLCL*-Filter under Wide Variation of Grid-Reactance," *IEEE Transactions on Power Electronics*, vol. 34, no. 5, pp. 4362-4374, May 2019.

[41] A. Riccobono and E. Santi, "A novel passivity-based stability criterion (PBSC) for switching converter DC distribution systems," in *Proc. 2012 IEEE Applied Power Electronics Conference and Exposition (APEC)*, 2012, pp. 2560–2567.

Jintao Lei was born in Zhejiang, China. He received the B.S. degree in electrical engineering in 2018 from the College of Electrical Engineering, Zhejiang University, Hangzhou, China, where he is currently working toward the Ph.D. degree in electrical engineering at the College of Electrical Engineering.

Zian Qin (M'15-SM'19) received the B.Eng. degree in Automation from Beihang University, Beijing, China, in 2009, M.Eng. degree in Control Science and Engineering from Beijing Institute of Technology, Beijing, China, in 2012, and Ph.D. degree from Aalborg University, Aalborg, Denmark, in 2015.

He is currently an Assistant Professor in Delft University of Technology, Delft, Netherlands. In 2014, he was a Visiting Scientist at Aachen University, Aachen, Germany. From 2015 to 2017, he was a Postdoctoral Research Fellow in Aalborg University. His research interests include wide bandgap devices, power electronics based grid and Power2X. He serves as the technical programm chair of IEEE-ISIE 2020, technical program co-chair of IEEE-COMPEL 2020, industrial session co-chair of ECCE-Asia 2020.

Wuhua Li (M'09) received the B.Sc. and Ph.D. degree in Power Electronics and Electrical Engineering from Zhejiang University, Hangzhou, China, in 2002 and 2008, respectively.

From 2004 to 2005, he was a Research Intern, and from 2007 to 2008, a Research Assistant in GE Global Research Center, Shanghai, China. From 2008 to 2010, he joined the College of Electrical Engineering, Zhejiang University as a Post doctor. In 2010, he was promoted as an Associate Professor. Since 2013, he has been a Full Professor at Zhejiang University. From 2010 to 2011, he was a Ryerson University Postdoctoral Fellow with the Department of Electrical and Computer Engineering, Ryerson University, Toronto, ON, Canada. He is currently the Executive Deputy Director of the National Specialty Laboratory for Power Electronics and the Vice Director of the Power Electronics Research Institute, Zhejiang University. His research interests include power devices, converter topologies and advanced controls for high power energy conversion systems. Dr. Li has published more than 300 peer-reviewed technical papers and holds over 50 issued/pending patents.

Due to his excellent teaching and research contributions, Dr. Li received the 2012 Delta Young Scholar from Delta Environmental & Educational Foundation, 2012 Outstanding Young Scholar from National Science Foundation of China (NSFC), 2013 Chief Youth Scientist of National 973 Program, 2014 Young Top-Notch Scholar of National Ten Thousand Talent Program, 2019 Distinguished Young Scholar from National Science Foundation of China. He serves as the Associated Editor of Journal of Emerging and Selected Topics in Power Electronics, IET Power Electronics, CSEE Journal of Power and Energy Systems, CPSS Transactions on Power Electronics and Applications, Proceedings of the Chinese Society for Electrical Engineering, Guest Editor of IET Renewable Power Generation for Special Issue "DC and HVDC system technologies", Member of Editorial Board for Journal of Modern Power System and Clean Energy.

He received one National Natural Science Award and four Scientific and Technological Achievement Awards from Zhejiang Provincial Government and the State Educational Ministry of China. He was appointed as the Most Cited Chinese Researchers by Elsevier since 2014.

Pavol Bauer (SM'07) is currently a full Professor with the Department of Electrical Sustainable Energy of Delft University of Technology and head of DC Systems, Energy Conversion and Storage group. He received Masters in Electrical Engineering at the Technical University of Kosice (a85), Ph.D. from Delft University of Technology (a95) and title prof. from the president of Czech Republic at the Brno University of Technology (2008) and Delft University of Technology (2016). He published over 72 journal and almost 300 conference papers in my field (with H factor Google scholar 43, Web of science 20), he is an author or co-author of 8 books, holds 4 international patents and organized several tutorials at the international conferences. He has worked on many projects for industry concerning wind and wave energy, power electronic applications for power systems such as Smarttrafo; HVDC systems, projects for smart cities such as PV charging of electric vehicles, PV and storage integration, contactless charging; and he participated in several Leonardo da Vinci and H2020 EU projects as project partner (ELINA, INETELE, E-Pragmatic) and coordinator (PEMCWebLab.com-Edipe, SustEner, Eranet DCMICRO).

Xiangning He (M'95--SM'96--F'10) received the B.Sc. and M.Sc. degrees from Nanjing University of Aeronautical and Astronautical, Nanjing, China, in 1982 and 1985, respectively, and the Ph.D. degree from Zhejiang University, Hangzhou, China, in 1989.

From 1985 to 1986, he was an Assistant Engineer at the 608 Institute of Aeronautical Industrial General Company, Zhuzhou, China. From 1989 to 1991, he was a Lecturer at Zhejiang University. In 1991, he obtained a Fellowship from the Royal Society of U.K., and conducted research in the Department of Computing and Electrical Engineering, Heriot-Watt University, Edinburgh, U.K., as a Post-Doctoral Research Fellow for two years. In 1994, he joined Zhejiang University as an Associate Professor. Since 1996, he has been a Full Professor in the College of Electrical Engineering, Zhejiang University. He was the Director of the Power Electronics Research Institute, the Head of the Department of Applied Electronics, the Vice Dean of the College of Electrical Engineering, and he is currently the Director of the National Specialty Laboratory for Power Electronics, Zhejiang University. His research interests are power electronics and their industrial applications.

Dr. He is a Fellow of The Institute of Electrical and Electronics Engineers (IEEE) and was appointed as IEEE Distinguished Lecturer by the IEEE Power Electronics Society 2011--2015. He is also a Fellow of the Institution of Engineering and Technology (formerly IEE), U.K.